

DESY 97-251  
December 1997

arXiv:hep-ph/9712415v2 19 Aug 2004

# The ALLM parameterization of $\sigma_{tot}(\gamma^*p)$ an update

**H. Abramowicz and A. Levy**

*School of Physics and Astronomy*

*Raymond and Beverly Sackler Faculty of Exact Sciences*

*Tel-Aviv University, Tel-Aviv, Israel*

## **Abstract**

The ALLM parameterization of  $\sigma_{tot}(\gamma^*p)$  has been updated by using all published  $F_2$  data to determine its parameters. The fit yields a  $\chi^2/\text{ndf}$  of 0.97 for the 1356 data points. The updated ALLM parameterization, ALLM97, gives a good description of all the available data in the whole  $x$  and  $Q^2$  range studied so far ( $3 \times 10^{-6} < x < 0.85$ ,  $0 \leq Q^2 < 5000 \text{ GeV}^2$ ).

# 1 Introduction

The ALLM (Abramowicz, Levin, Levy, Maor) parameterization [1] is a parameterization for describing the total  $\gamma^*p$  cross section,  $\sigma_{tot}(\gamma^*p)$ , above the resonance region in the whole  $Q^2$  range, where  $Q^2$  is the negative of the four-momentum transfer squared of the exchanged photon in  $ep$  interactions. It is constructed so as to include also the real photon ( $Q^2 = 0$ ) cross section. There were two main reasons for such a parameterization. The practical reason was that it was needed for estimating acceptance corrections and radiative corrections in the whole  $Q^2$  region for  $W^2 > 3 \text{ GeV}^2$ , where  $W$  is the  $\gamma^*p$  center of mass energy. The theoretical reason was the hope that it would shed light on the transition region between the soft and hard interactions and their interplay.

The parameterization is based on a Regge motivated approach, similar to that used earlier by Donnachie and Landshoff [2], extended into the large  $Q^2$  regime in a way compatible with QCD expectations. The data used to fit the parameters were all the  $F_2$  measurements available in 1991 together with the total photoproduction cross section data, which were measured at that time up to center of mass energies of  $W \approx 20 \text{ GeV}$ . In spite of the fact that the fit used relatively high Bjorken  $x$  data and data of  $\sigma_{tot}(\gamma p)$  at low energies, its predictions agreed amazingly well with the new HERA data, both for real and virtual photon cross sections. This can be seen in figure 1 which shows the total  $\gamma^*p$  cross section as function of the center of mass energy squared,  $W^2$ , for fixed  $Q^2$  values [3]. The curves are the ALLM parameterization which were fitted to the lower energy data ( $W^2 < 400 \text{ GeV}^2$ ) and extrapolated to the first HERA measurements. The predictions did very well for the photoproduction data as well as for the  $Q^2 > 30 \text{ GeV}^2$  region. However, at low  $x$ , in the intermediate  $5 < Q^2 < 25 \text{ GeV}^2$  region the predictions turned out to be higher than the data.

An attempt was made in 1995 to include the first HERA  $F_2$  data in the fit. The new parameterization, ALLM-N [4], did somewhat better in the region of  $Q^2 \approx 10 \text{ GeV}^2$ , as can be seen in figure 2, but was not quite satisfactory in the low  $Q^2$  region.

The purpose of this note is to describe the results of a further update of the ALLM parameterization, to be denoted ALLM97, where all available published data of  $F_2$ , including the very low  $x$ , low  $Q^2$  data are used. As will be shown, this parameterization gives an excellent description of all the data and can reproduce features like the slope in  $Q^2$  and in  $x$ , where all other parameterizations fail. It can be used in the whole  $x$  and  $Q^2$  region above the resonance region ( $W^2 > 3 \text{ GeV}^2$ ).

## 2 The ALLM parameterization - a short recap

The proton structure function is assumed to have the form

$$F_2(x, Q^2) = \frac{Q^2}{Q^2 + m_0^2} \left( F_2^{\mathcal{P}}(x, Q^2) + F_2^{\mathcal{R}}(x, Q^2) \right), \quad (1)$$

where  $m_0$  is the effective photon mass. The functions  $F_2^{\mathcal{P}}$  and  $F_2^{\mathcal{R}}$  are the contributions of the Pomeron  $\mathcal{P}$  or Reggeon  $\mathcal{R}$  exchanges to the structure function. They take the form

$$\begin{aligned} F_2^{\mathcal{P}}(x, Q^2) &= c_{\mathcal{P}}(t) x_{\mathcal{P}}^{a_{\mathcal{P}}(t)} (1-x)^{b_{\mathcal{P}}(t)}, \\ F_2^{\mathcal{R}}(x, Q^2) &= c_{\mathcal{R}}(t) x_{\mathcal{R}}^{a_{\mathcal{R}}(t)} (1-x)^{b_{\mathcal{R}}(t)}. \end{aligned} \quad (2)$$

The slowly varying function  $t$  is defined as

$$t = \ln \left( \frac{\ln \frac{Q^2 + Q_0^2}{\Lambda^2}}{\ln \frac{Q^2}{\Lambda^2}} \right), \quad (3)$$

where  $\Lambda$  is the QCD scale and  $Q_0^2$  is a parameter.

The two scaled variables  $x_{\mathcal{P}}$  and  $x_{\mathcal{R}}$  are modified Bjorken- $x$  variables which include mass parameters  $m_{\mathcal{P}}$  and  $m_{\mathcal{R}}$ , interpreted as effective Pomeron and reggeon masses:

$$\begin{aligned} \frac{1}{x_{\mathcal{P}}} &= 1 + \frac{W^2 - M^2}{Q^2 + m_{\mathcal{P}}^2}, \\ \frac{1}{x_{\mathcal{R}}} &= 1 + \frac{W^2 - M^2}{Q^2 + m_{\mathcal{R}}^2}. \end{aligned} \quad (4)$$

where  $M$  is the proton mass. The scale parameters  $m_0^2, m_{\mathcal{P}}^2, m_{\mathcal{R}}^2$ , and  $Q_0^2$ , allow a smooth transition to  $Q^2 = 0$  values. For large  $Q^2$ ,  $Q^2 \gg m_{\mathcal{P}}^2, Q^2 \gg m_{\mathcal{R}}^2$ , the scaled  $x_{\mathcal{P}}$  and  $x_{\mathcal{R}}$  variables approach Bjorken  $x$ .

Four of the six parameters in equation 2,  $c_{\mathcal{R}}, a_{\mathcal{R}}, b_{\mathcal{R}}$  and  $b_{\mathcal{P}}$  increase with  $Q^2$  as

$$f(t) = f_1 + f_2 t^c \quad (5)$$

while the remaining two,  $c_{\mathcal{P}}$  and  $a_{\mathcal{P}}$  decrease with  $Q^2$  like:

$$g(t) = g_1 + (g_1 - g_2) \left[ \frac{1}{1 + t^d} - 1 \right]. \quad (6)$$

There are altogether 23 parameters to be determined from a fit to the data. Note that about half of the parameters are needed for the description of the low  $W$  (high  $x$ ) region where higher twist effects are important.

The data used in the first fit (ALLM91) were all data available from the pre-HERA era, which resulted in 694 data points. These included the low energy data of  $\sigma_{tot}(\gamma p)$  [5], and the  $F_2$  data of the SLAC [6], BCDMS [7], and NA28 [8] collaborations. The best fit to the data had a  $\chi^2/\text{ndf}=0.98$ .

As stated in the introduction and shown in figure 1, the predictions of the parameterization ALLM91 to the first HERA data were in agreement with the measurements at  $Q^2=0$  and in the higher  $Q^2$  region. Though some of the low  $x$  parameters were constrained by the NA28 measurements, the intermediate  $Q^2$  region was not well described, mainly due to the fact that the  $Q^2$  dependence of the Pomeron intercept,  $\alpha_{\mathcal{P}}(Q^2)$ , shown in figure 3, came out too steep in the first fit.

The inclusion of the first HERA measurements as well as the preliminary NMC data yielded the parameterization ALLM-N, which produced a milder  $Q^2$  transition of the Pomeron intercept, but fails to describe the latest low  $x$  low  $Q^2$  data. This prompted a third attempt to determine the parameters including the latest data, as described in the next section.

### 3 The data sample for ALLM97

The following data have been used for the present fit. All fixed target photoproduction total cross section data were used together with those of H1 [9] and ZEUS [10] in the HERA region, a total of 228 data points. The  $F_2$  structure function data of the following fixed target collaborations: SLAC (211 points), BCDMS (177), E665 (87) [11], and NMC (158) [12]. From the HERA  $ep$  collider we used the H1-94 data (193 points) [13], H1 low  $Q^2$  data (44) [14], the ZEUS shifted vertex data (36) [15], ZEUS-94 (188) [16] and the very low  $Q^2$  ZEUS data measured with a beam pipe calorimeter (BPC) (34 data points) [17]. Altogether 1356 data points were used in the fit resulting in a  $\chi^2/\text{ndf}=0.97$ . The contribution of each data sample to the  $\chi^2$  is given in table 1.

Data set	# of points	$\chi^2$
$\gamma p$ [5], [9], [10]	228	262.3
SLAC [6]	211	171.2
BCDMS [7]	177	168.1
E665 [11]	87	95.7
NMC [12]	158	142.0
H1-94 [13]	193	127.1
H1(Low $Q^2$ ) [14]	44	34.4
ZEUS(SVX) [15]	36	26.7
ZEUS-94 [16]	188	253.8
ZEUS(BPC) [17]	34	17.3
Total	1356	1298.7
$\chi^2/\text{ND}$		0.97

**Table 1:** Data used in the ALLM97 fit, with the  $\chi^2$  contribution of each set.

## 4 Results

The resulting parameter values of the ALLM97 fit are compared in table 2 to their values from the ALLM91 fit. The biggest difference can be seen in the value of the scale parameter of the Pomeron which increased by almost a factor of 5. This increase affects the shape of the transition region in the low  $x$  low  $Q^2$  region. This can be seen in figure 4 where the dependence of the Pomeron intercept on  $Q^2$  is plotted for the old (ALLM91) and the new (ALLM97) parameterization. The latter allows for an early start of the transition from the soft to the hard regime. Note that in the present fit the intercept at  $Q^2=0$  was fixed to the Donnachie-Landshoff (DL) [18] value since the total photoproduction measurements in the HERA region do not allow a precise determination of this value.

### 4.1 $F_2$ as function of $Q^2$

The  $F_2$  data [19] used in the fit are displayed in figure 5 as function of  $Q^2$  for fixed  $x$  intervals, together with the results of the ALLM97 parameterization. One sees the well known scaling

Parameter	ALLM91	ALLM97
$m_0^2(\text{GeV}^2)$	0.30508	0.31985
$m_P^2(\text{GeV}^2)$	10.676	49.457
$m_R^2(\text{GeV}^2)$	0.20623	0.15052
$Q_0^2(\text{GeV}^2)$	0.27799	0.52544
$\Lambda^2(\text{GeV}^2)$	0.06527	0.06527
$c_{P1}$	0.26550	0.28067
$c_{P2}$	0.04856	0.22291
$c_{P3}$	1.04682	2.1979
$a_{P1}$	-0.04503	-0.0808
$a_{P2}$	-0.36407	-0.44812
$a_{P3}$	8.17091	1.1709
$b_{P1}$	0.49222	0.36292
$b_{P2}$	0.52116	1.8917
$b_{P3}$	3.5515	1.8439
$c_{R1}$	0.67639	0.80107
$c_{R2}$	0.49027	0.97307
$c_{R3}$	2.66275	3.4942
$a_{R1}$	0.60408	0.58400
$a_{R2}$	0.17353	0.37888
$a_{R3}$	1.61812	2.6063
$b_{R1}$	1.26066	0.01147
$b_{R2}$	1.83624	3.7582
$b_{R3}$	0.81141	0.49338

**Table 2:** *The parameter values in the old (ALLM91) and new (ALLM97) parameterization.*

violation behaviour of the data, being positive for low  $x$  values and turning negative in the high  $x$  region.

The curves in the figure are the results of the ALLM97 parameterization and are seen to go through most of the data in the whole  $(x, Q^2)$  region. This reflects the good  $\chi^2$  obtained from the fit.

## 4.2 $\sigma_{tot}$ as function of $Q^2$

The H1 collaboration [14] presented their results together with those of the ZEUS BPC data as an effective virtual photon-proton cross section,  $\sigma_{\gamma^*p}^{eff}$ , as function of  $Q^2$  for fixed  $W$  intervals. The effective cross section is given by  $\sigma_{\gamma^*p}^{eff} = \sigma_T + \epsilon\sigma_L$ , where  $\sigma_T$  and  $\sigma_L$  are the cross sections for transverse and longitudinally polarized virtual photons and  $\epsilon$  is the ratio of longitudinal to transverse flux. The data are displayed in figure 6. Since in the HERA kinematic region  $\epsilon \approx 1$ , the data are compared to the old (ALLM-N) and new (ALLM97) parameterization of  $\sigma_{tot}(\gamma^*p)$ . The ALLM97 parameterization gives a good description of the data. Also shown are the two points at  $Q^2=0$  which are also well described by the new parameterization.

### 4.3 $\sigma_{tot}$ as function of $W^2$

The  $F_2$  data can be converted to  $\sigma_{tot}(\gamma^*p)$  using the relation

$$\sigma_{tot}(\gamma^*p) = \frac{4\pi^2\alpha}{Q^2(1-x)} \frac{Q^2 + 4M^2x^2}{Q^2} F_2(W^2, Q^2). \quad (7)$$

The  $F_2$  data at low  $Q^2$ , starting as low as  $Q^2=0.11$  GeV<sup>2</sup>, are shown in figure 7 in the form of  $\sigma_{tot}(\gamma^*p)$  together with the real photon total cross sections. The data are compared to expectations of different parameterizations. While the Donnachie–Landshoff (DL) parameterization agrees well with  $\sigma_{tot}(\gamma p)$ , its predictions are lower than the data once  $Q^2 \neq 0$ , with the disagreement increasing with  $Q^2$ . The GRV [20] parameterization is plotted starting at  $Q^2 = 0.65$  GeV<sup>2</sup>, where it lies below the data, while at higher  $Q^2$  values the predictions are above the data. The ALLM97 parameterization agrees with the data at all  $Q^2$  values.

The good agreement of the ALLM97 parameterization in the whole accessible kinematic region at present can be seen in figure 8 where the total cross section is plotted in the range  $0 \leq Q^2 \leq 2000$  GeV<sup>2</sup>. It gives a good description of the data at high as well as at low  $W^2$ .

In order to compare the results of the ALLM97 parameterization to that of a recent QCD evolution type of parameterization, we show in the same figure also the MRSR1 [21] parameterization which is valid for  $Q^2 > 1.25$  GeV<sup>2</sup>. The two parameterizations agree well with each other for  $Q^2 \geq 10$  GeV<sup>2</sup>, while at lower  $Q^2$  values the MRSR1 parameterization has a shallower  $W^2$  dependence and thus is lower than the data.

## 5 The transition region

The different  $W^2$  behaviour of the high  $Q^2$  data and at  $Q^2=0$  prompted the measurements of deep inelastic  $ep$  reactions in the low  $Q^2$  region in order to find where the transition takes place. We will look at two ways of studying this question. One is by looking at the change in the slope of  $F_2$  with respect to  $\ln Q^2$  and the other is to study  $d \ln F_2 / d \ln x$ , both of which are discussed below.

### 5.1 $dF_2/d \ln Q^2$ as function of $x$ for some $Q^2$ values

The scaling violation of  $F_2$  is expected to increase as  $x$  gets smaller according to QCD. This feature is also borne out by the data as shown in figure 5. One can quantify this by looking at the change of the slope of  $F_2$  with respect to  $\ln Q^2$  for different  $x$  values. Once the non-perturbative processes take over, as expected at low  $Q^2$ , one should see a change in the slope. The place where the change occurs would indicate the transition from soft to hard physics.

The distribution of  $dF_2/d \ln Q^2$  as function of  $x$  [22] is shown for the HERA data in figure 9 for  $Q^2$  values ranging from about 1000 GeV<sup>2</sup> down to 0.13 GeV<sup>2</sup>. Some values are given at the top of the figure. The HERA data include the H194, H1 low  $Q^2$ , ZEUS94, ZEUS shifted vertex and ZEUS BPC data. As expected, the slope rises as  $x$  decreases down to  $x \approx 10^{-4}$ . However for lower  $x$  there is a change in the tendency of the slope which becomes smaller as  $x$  decreases.

This happens at  $Q^2$  values of about 1-2 GeV<sup>2</sup>. Note that as  $x$  decreases also  $Q^2$  decreases. In the same figure we plot for comparison the expectation of the GRV parameterization. This parameterization starts its evolution at  $Q^2 \approx 0.4$  GeV<sup>2</sup>. While the parameterization shows the same features as the data for  $Q^2 > 5$  GeV<sup>2</sup>, it continues to rise with  $x$  also below  $x = 10^{-4}$ , contrary to the data. Judging from the GRV distribution, the turnover point starts as high as  $Q^2 \approx 4$  GeV<sup>2</sup>.

Another way of trying to find the turning point is to compare the same data to another QCD evolution type parameterization and to a Regge based one. This is done in figure 10, where the data are compared to the results of the MRSR1 parameterization and to the expectations from a Regge fit which was done [23] to the BPC data. The MRSR1 parameterization start its evolution at  $Q^2 = 1.25$  GeV<sup>2</sup>, where it is higher than the data until about  $Q^2 \approx 3-4$  GeV<sup>2</sup> from whereon it follows the data. The Regge fit starts from the lowest  $Q^2$  point and agrees with the data up to about  $Q^2 = 1$  GeV<sup>2</sup>, but continues to rise at higher  $Q^2$  values contrary to the data. The QCD and Regge results cross at  $Q^2 \approx 2$  GeV<sup>2</sup>. One could thus conclude from here that the transition region is in the region of 1 - 3 GeV<sup>2</sup>.

Finally, in figure 11 the data are compared to the ALLM97 parameterization. One observes good agreement between the parameterization and the data. Thus one does not need to use two different parameterizations to describe the low  $Q^2$  soft and the high  $Q^2$  hard regimes. ALLM97 gives a good parameterization of both regimes.

## 5.2 $d \ln F_2/d \ln x$ as function of $Q^2$

The slope of  $d \ln F_2/d \ln x$  can be related to the Pomeron intercept. In the low  $x$  region,  $F_2$  is behaving like  $x^{-\lambda}$ , where  $\lambda$  is a function of  $Q^2$ . Since for fixed  $Q^2$ ,  $W^2 \sim x^{-1}$ ,  $\sigma_{tot}(\gamma^*p) \sim W^{2\lambda}$  and therefore  $\lambda = \alpha_P - 1$ . Therefore, measuring  $d \ln F_2/d \ln x$  as function of  $Q^2$  is equivalent to measuring  $\lambda$ . When making this interpretation it is crucial to choose the right  $x$  region from which the slope is determined.

This last point is demonstrated in figure 12 where the slope  $\lambda$  as function of  $Q^2$  is shown for different  $x$  cuts, as indicated in the figure, for the separate data sets of each experiment. Note that in order to obtain  $\lambda$  at a fixed  $Q^2$ , a minimum of 4 data points at different  $x$  values were required. The full line is  $\alpha_P - 1$  as calculated from the ALLM97 parameterization, where  $\alpha_P$  is the Pomeron intercept, and the dashed line gives the value of  $\lambda$  obtained from the parameterization in the same procedure as that applied to the data. As one sees, as long as one uses data in the very low  $x$  region,  $x < 10^{-3}$ , one can correlate the measured slope  $\lambda$  with the Pomeron intercept. For larger  $x$  cuts  $\lambda$  may not be always a good estimate of  $\alpha_P - 1$ , as shown for example for  $x < 0.05$ . The NMC data in the low  $Q^2$  region do not reach very low  $x$  values, their lowest being  $x=0.0045$ , and thus produce low  $\lambda$  results. The HERA data in the region  $Q^2 > 200$  GeV<sup>2</sup> overestimate the Pomeron intercept by determining the slope in a narrow  $x$  region, typically  $0.01 < x < 0.05$ . These effects are reproduced by the ALLM97 parameterization.

## 6 Summary and conclusions

The ALLM parameterization has been updated by using all the published data to determine its parameters leading to ALLM97. A very good description of the data in the whole  $(x, Q^2)$

kinematic region is obtained, including the  $Q^2 = 0$  photoproduction measurements down to  $W^2 = 3 \text{ GeV}^2$  and the low  $Q^2$  and low  $x$  region where the transition from soft to hard processes is observed in the data.

We have hereby demonstrated that it is possible to find a functional form which describes the data in the whole of the kinematical region. Such a parameterization has many practical applications and in addition allows to study features of the data which are helpful for understanding the interplay between soft and hard processes.

## Acknowledgments

We would like to thank our colleagues Eugene Levin and Uri Maor for their continuous support in this study. We also thank Vladimir Chekelyan and Bernd Surrow for their help with some of the figures. The critical reading of the text by Guenter Wolf is highly appreciated.

This work was partially supported by the German–Israel Foundation (GIF) and the Israel Science Foundation.

## References

- [1] H. Abramowicz, E. Levin, A. Levy, U. Maor, *Phys. Lett.* **B269** (1991) 465.
- [2] A. Donnachie, P.V. Landshoff, *Nucl. Phys.* **B244** (1984) 322.
- [3] A. Levy, DESY 95–003 (1995).
- [4] A. Marcus, TAUP–2350 (1996).
- [5] D.O. Caldwell et al., *Phys. Rev. Lett.* **40** (1978) 1222;  
S.I. Alekhin et al., CERN–HERA 87–01 (1987).
- [6] L.W. Whitlow, SLAC–357 (1990).
- [7] BCDMS Collab., A.C. Benvenuti et al., *Phys. Lett.* **B223** (1989) 485.
- [8] NA28 Collab., M. Arneodo et al., *Nucl. Phys.* **B333** (1990) 1.
- [9] H1 Collab., S. Aid et al., *Zeit. Phys.* **C69** (1995) 27.
- [10] ZEUS Collab., M. Derrick et al., *Zeit. Phys.* **C63** (1994) 391.
- [11] E665 Collab., M.R. Adams et al., *Phys. Rev.* **D54** (1996) 3006.
- [12] NMC Collab., M. Arneodo et al., *Nucl. Phys.* **B483** (1997) 3.
- [13] H1 Collab., S. Aid et al., *Nucl. Phys.* **B470** (1996) 3.
- [14] H1 Collab., C. Adloff et al., *Nucl. Phys.* **B497** (1997) 3.
- [15] ZEUS Collab., M. Derrick et al., *Zeit. Phys.* **C69** (1996) 607.



- [16] ZEUS Collab., M. Derrick et al., *Zeit. Phys.* **C72** (1996) 399.
- [17] ZEUS Collab., J. Breitweg et al., *Phys. Lett.* **B407** (1997) 432.
- [18] A. Donnachie, P. V. Landshoff, *Phys. Lett.* **B296** (1992) 227.
- [19] See e.g. H. Abramowicz, Rapporteur talk in *Proceedings of the XXVIII International Conference on High Energy Physics*, Warsaw, Poland, 1996.
- [20] M. Glück, E. Reya, A. Vogt, *Zeit. Phys.* **C67** (1995) 433.
- [21] A.D. Martin, R.G. Roberts, W.J. Stirling, *Phys. Lett.* **B387** (1996) 419.
- [22] A. Caldwell, Invited talk in the DESY Theory workshop, October 1997.
- [23] B. Surrow, private communication.

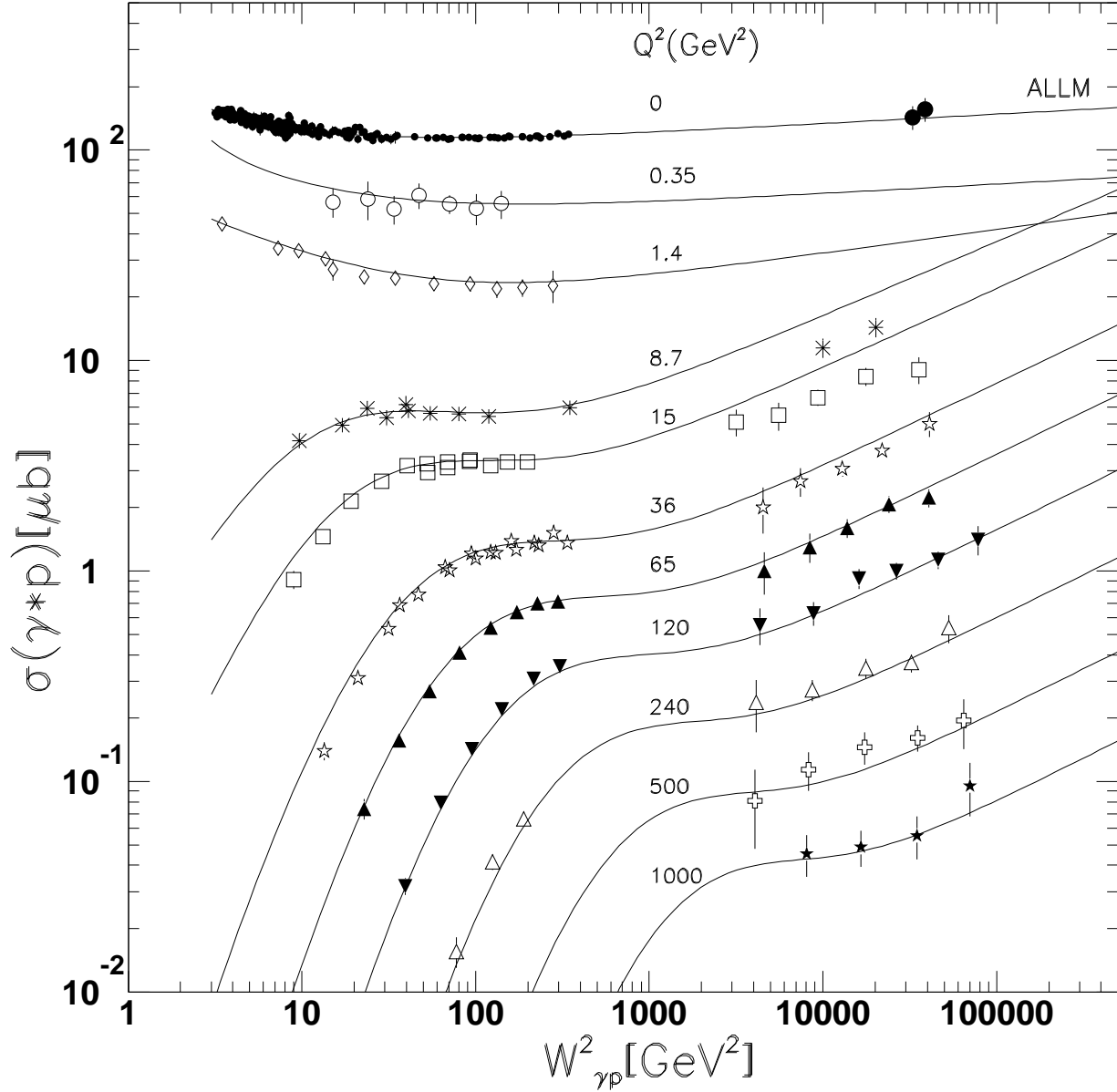


Figure 1: The total  $\gamma^*p$  cross section as function of  $W^2$ , for different  $Q^2$  values. The curves are the expectations of the ALLM parameterization.

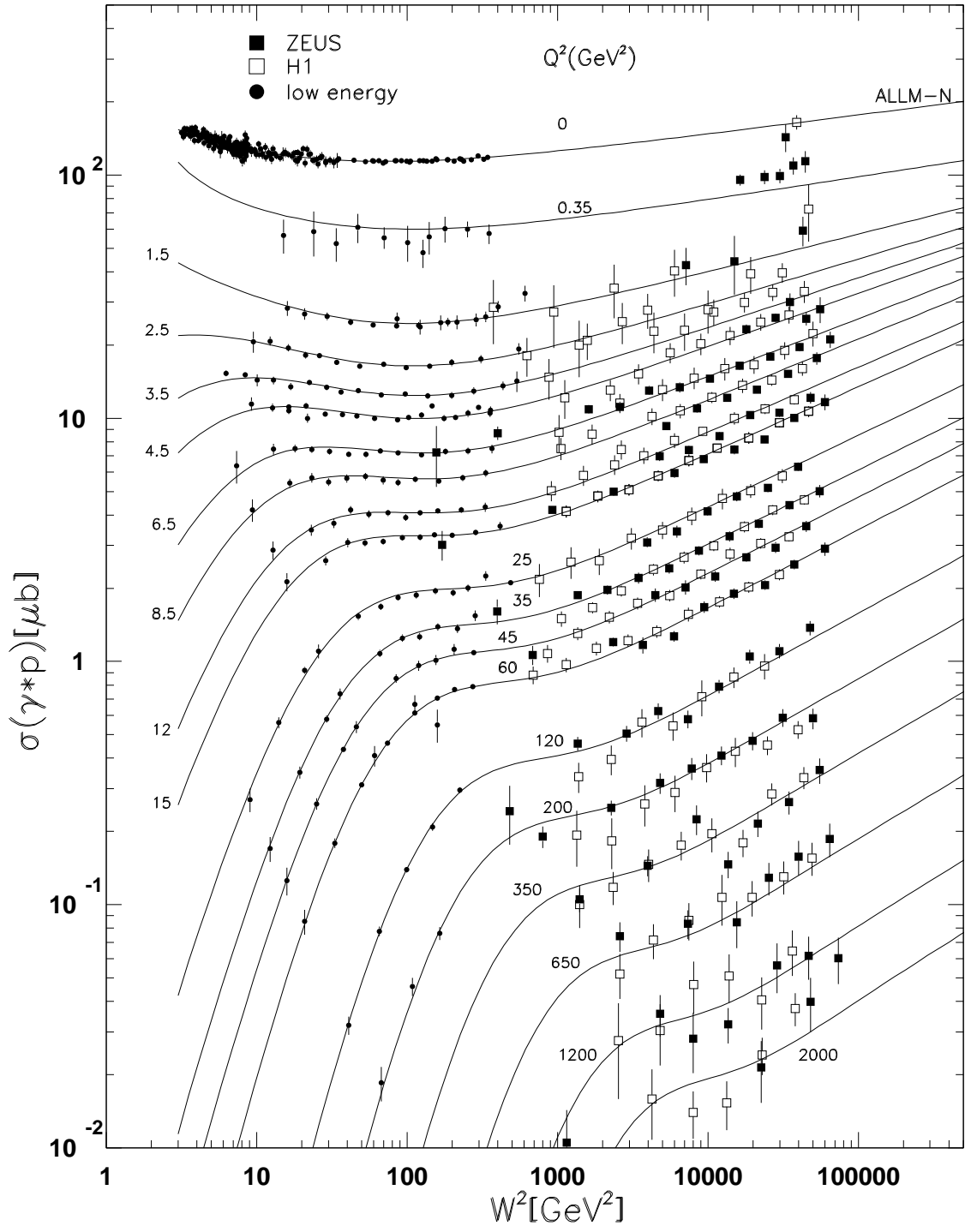


Figure 2: The total  $\gamma^*p$  cross section as function of  $W^2$ , for different  $Q^2$  values. The curves are the results of the ALLM-N parameterization.

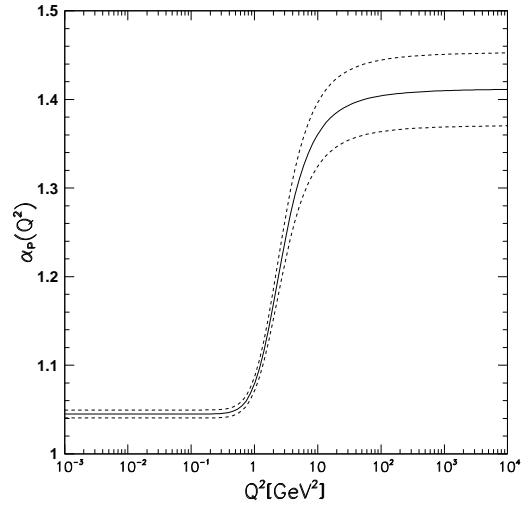


Figure 3: The intercept of the Pomeron trajectory as function of  $Q^2$ , as obtained from the ALLM parameterization. The dotted line shows the uncertainty of the fit.

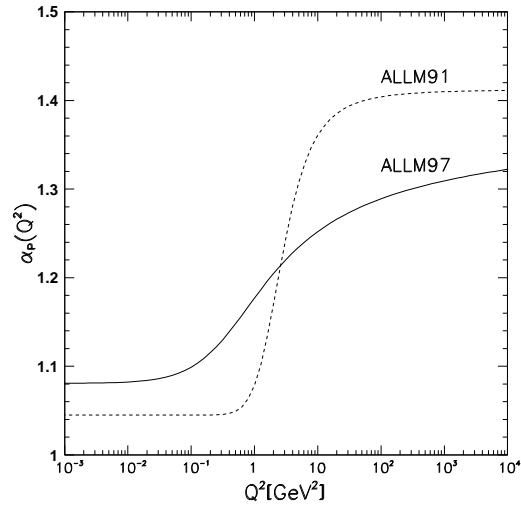


Figure 4: The intercept of the Pomeron trajectory as function of  $Q^2$ , as obtained from the ALLM97 (full line) and ALLM91 (dotted line) parameterizations.

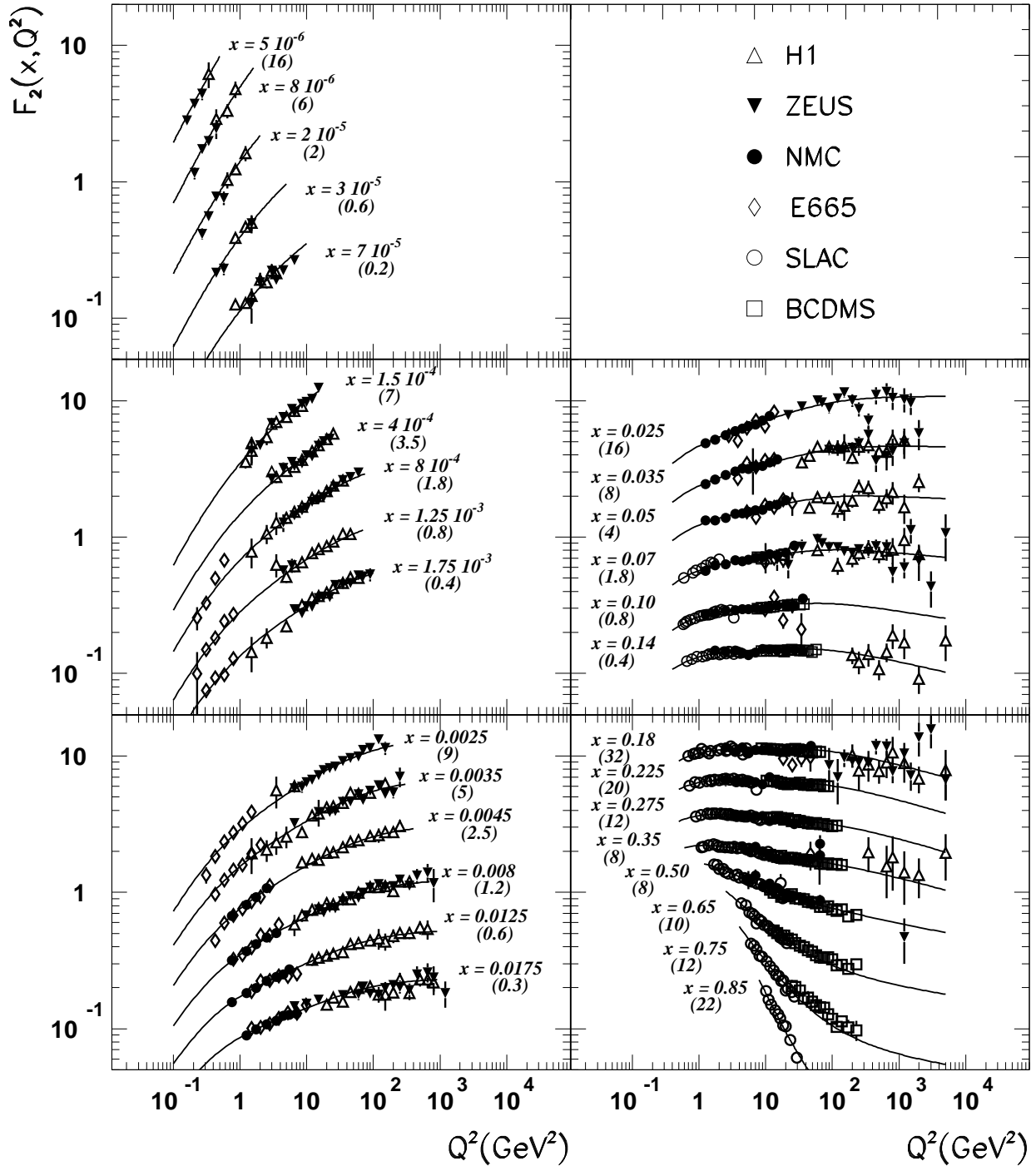


Figure 5: The dependence of the proton structure function,  $F_2(x, Q^2)$ , on  $Q^2$  for fixed  $x$  values as indicated in the figure. For display purposes, the structure function values have been scaled at each  $x$  by the factor shown in brackets under the  $x$  values. The curves are the results of the ALLM97 parameterization.

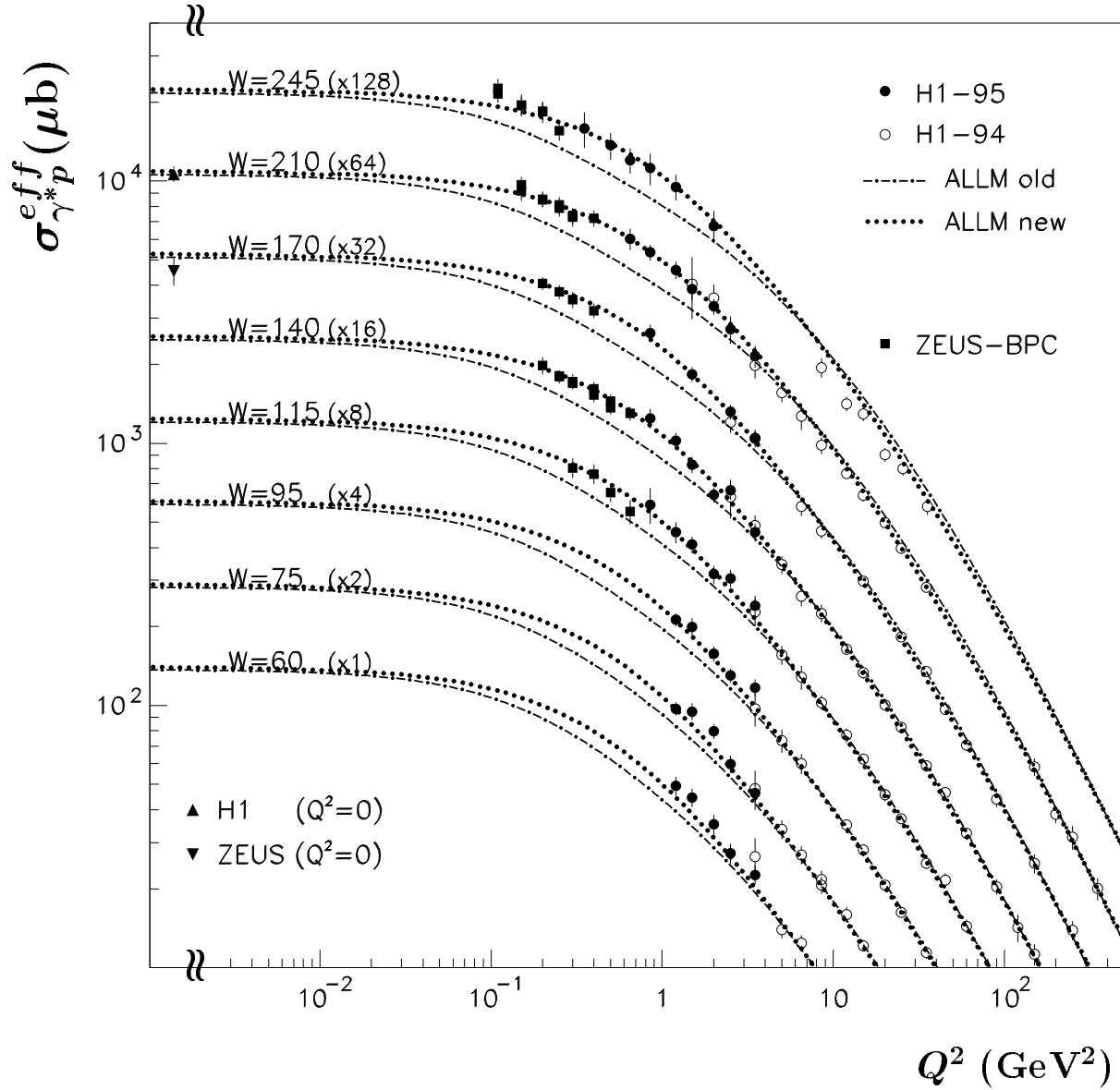


Figure 6: The effective virtual photon-proton cross section as function of  $Q^2$  for fixed  $W$  intervals. The full lines are the results of the ALLM97 parameterization and the dotted lines are those of the ALLM-N ones.

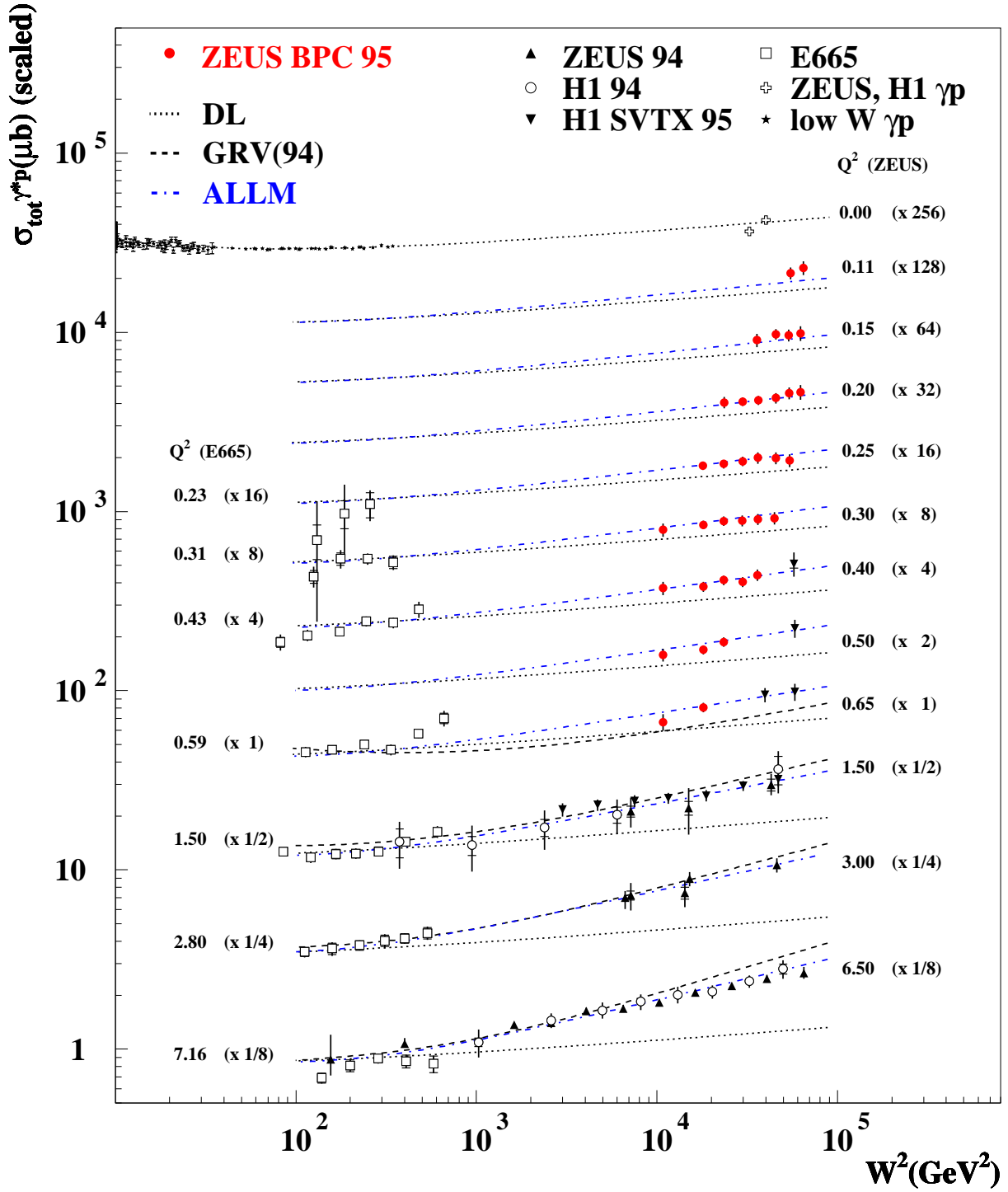


Figure 7: The total virtual photon-proton cross section as function of  $W^2$  for low  $Q^2$  data, scaled with the factors indicated in brackets for display purposes. The curves are the expectations of different parameterizations.

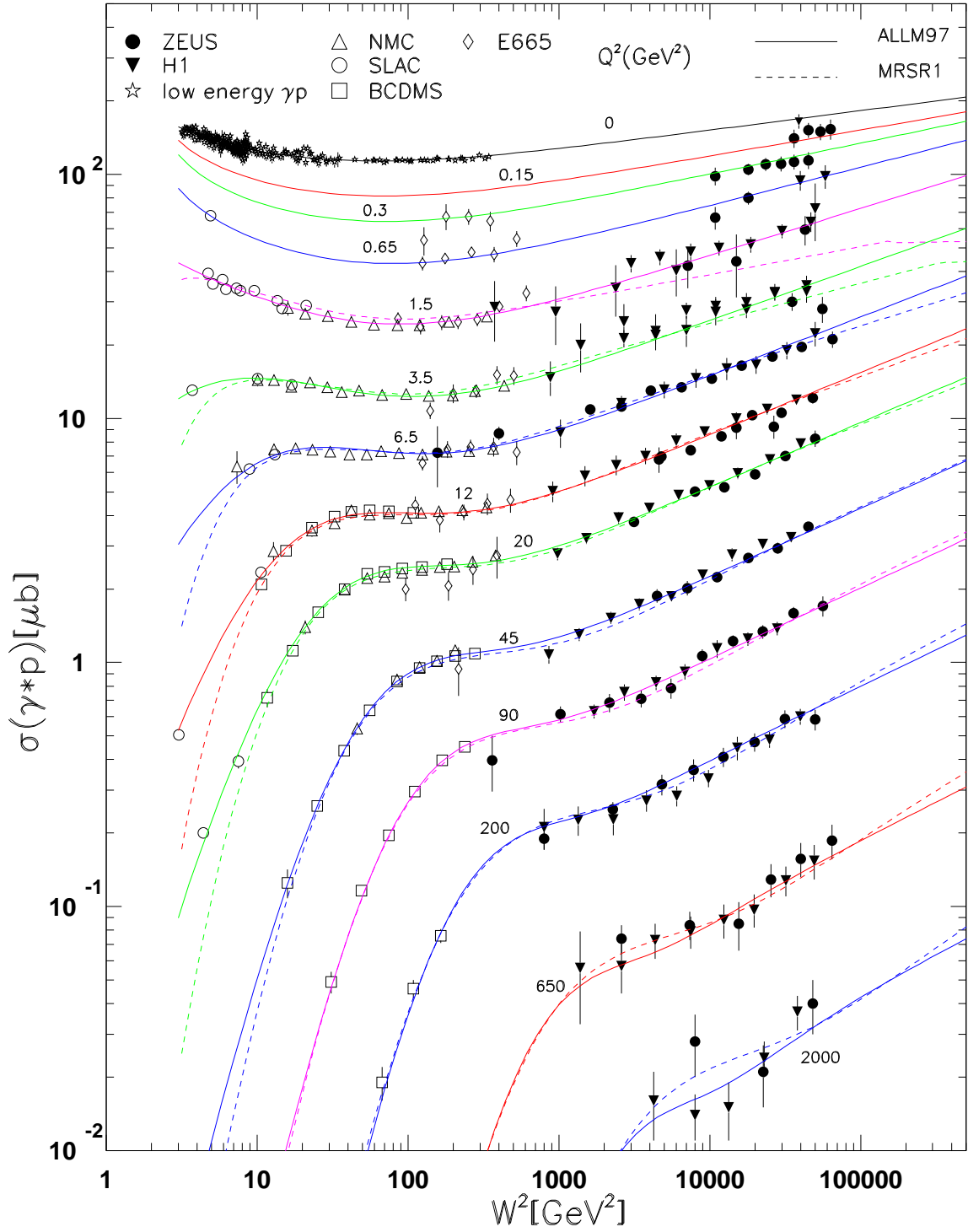


Figure 8: The total  $\gamma^*p$  cross section as function of  $W^2$ , for different  $Q^2$  values. The curves are the expectations of the ALLM97 parameterization (full line) and those of the MRSR1 one (dotted line).



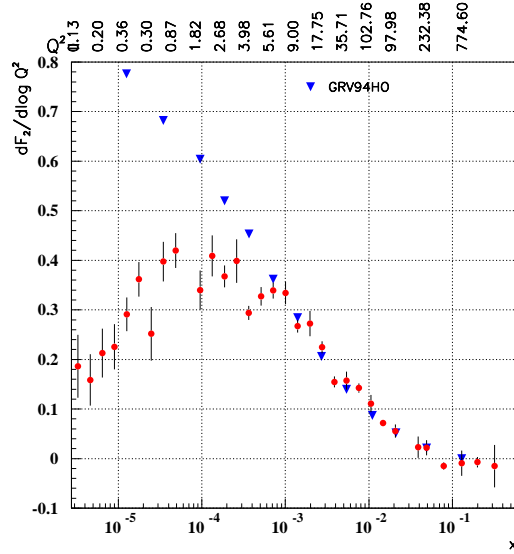


Figure 9: The slope of  $F_2$  with respect to  $\ln x$  as function of  $x$  for  $Q^2$  values as indicated in the figure. The round dots are the HERA data and the triangle symbols are the results of the GRV94HO parameterization.

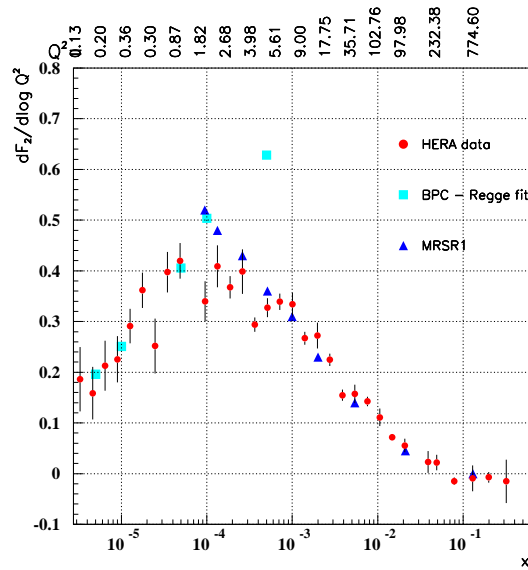


Figure 10: The slope of  $F_2$  with respect to  $\ln x$  as function of  $x$  for  $Q^2$  values as indicated in the figure. The round dots are the HERA data, the triangle symbols are the results of the MRSR1 parameterization and the full squares come from a Regge fit to the BPC data.

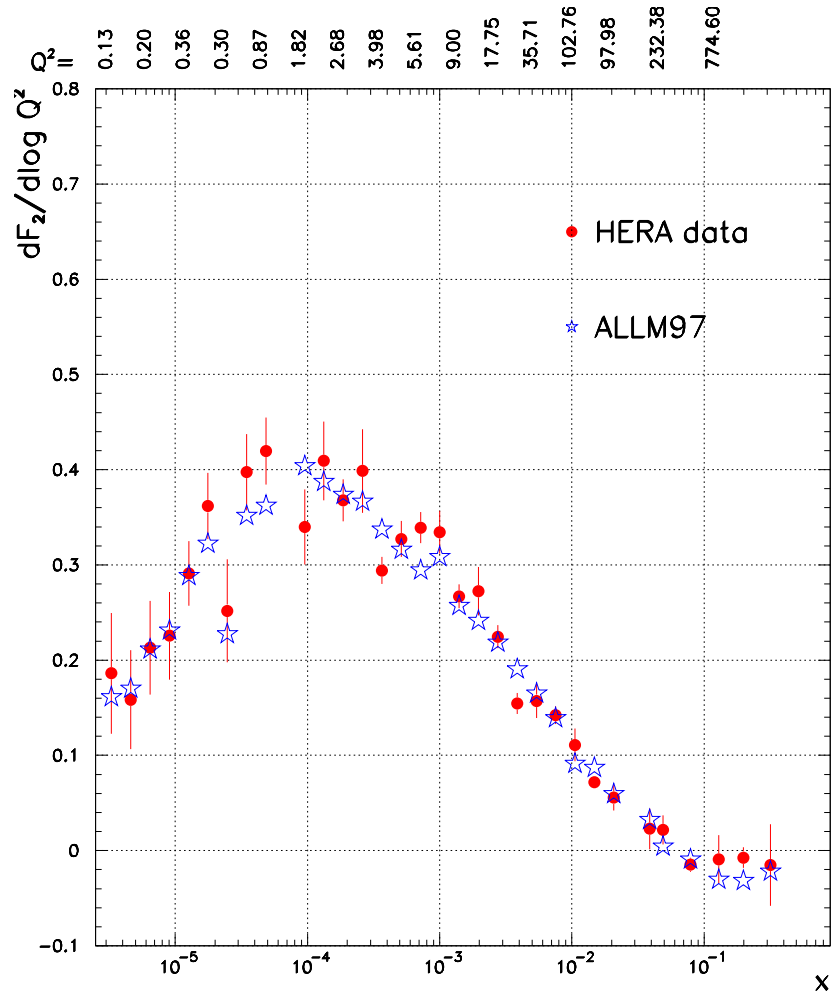


Figure 11: The slope of  $F_2$  with respect to  $\ln x$  as function of  $x$  for  $Q^2$  values as indicated in the figure. The full dots are the HERA data and the open symbols are the results of ALLM97.

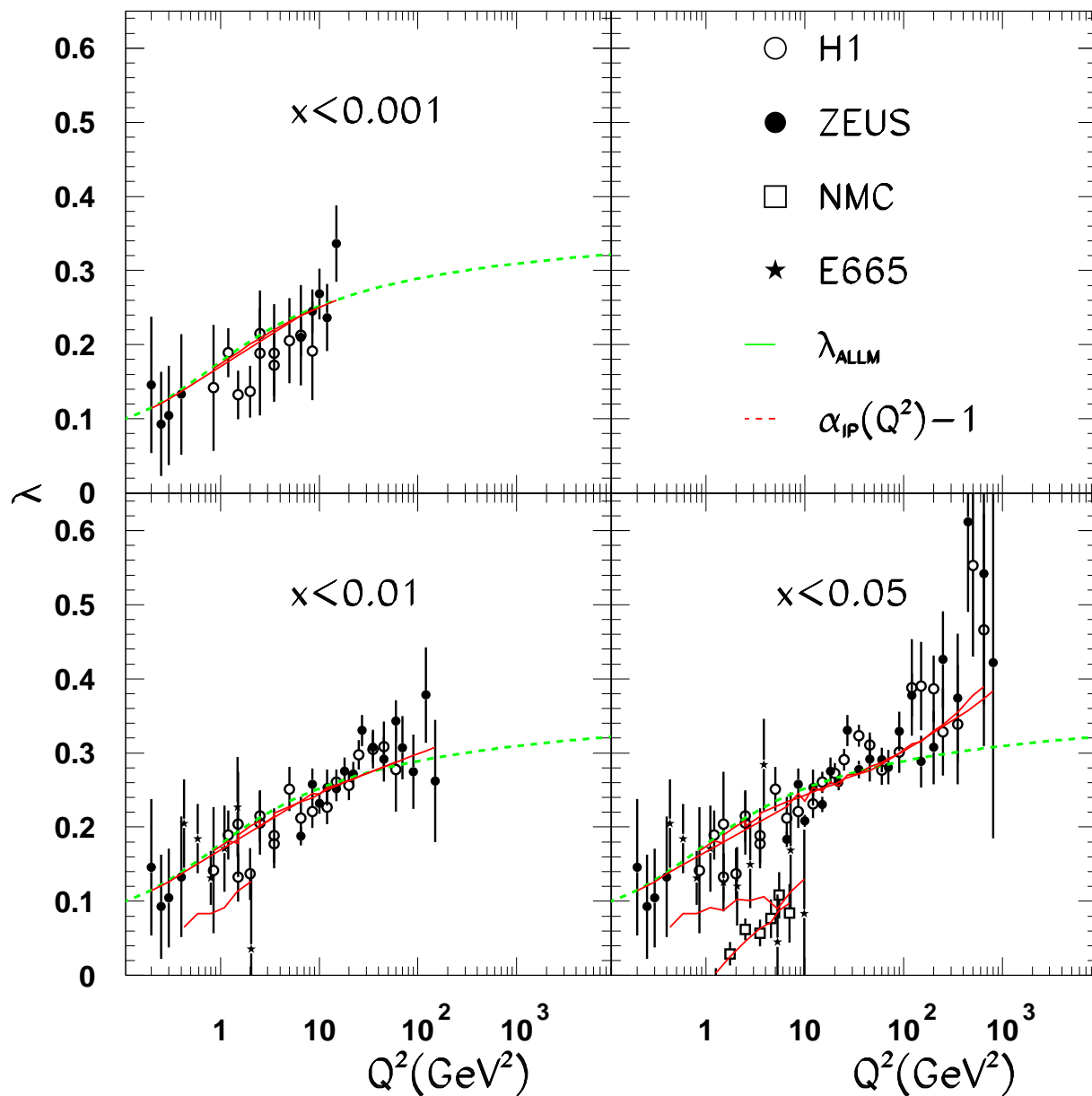


Figure 12: The slope  $\lambda$  as function of  $Q^2$  for different  $x$  cuts, as indicated in the figure. The dashed line is  $\alpha_P - 1$  as calculated from the ALLM97 parameterization, while the full line is the value of  $\lambda$  as obtained from the parameterization in the same way as from the data.